Design and Implementation of Robust Nonlinear Controller for Hybrid Power Sources with Considering Power Losses

Masoud Bahmanpour *, Hamid Reza Koofigar **‡, Majid Delshad ***, Mohammad Hasan Tosifian *

* Department of Electrical Engineering, Saveh Branch, Islamic Azad University, Saveh, Iran, 39197-15179

** Department of Electrical Engineering, University of Isfahan, Iran, 81746-73441

*** Department of Electrical Engineering, Isfahan Branch, Islamic Azad University, Isfahan, Iran, 81551- 39998

(m.bahmanpour@khuisf.ac.ir, koofigar@eng.ui.ac.ir, delshad@khuisf.ac.ir, Htosif@iau-saveh.ac.ir)

‡ Corresponding Author; Hamid Reza Koofigar, Department of Electrical Engineering, University of Isfahan, 81746-73441, Tel: +98 31 37934081, Fax: +98 31 37933071, koofigar@eng.ui.ac.ir

Received: 17.04.2018 Accepted:28.05.2018

Abstract- In this paper, the importance of taking into account power losses in the design of sliding mode controller (SMC) for hybrid power source (HPS) has been investigated. The underlying HPS consists of a boost converter, a bidirectional converter, a photovoltaic (PV) panel, and a battery. Dynamic equations of the system are derived based on the state-space averaging method. Afterward, a method to obtain power losses is provided. A robust control methodology, based on the SMC is then proposed to take the power losses into account. Asymptotic stability of the proposed method is ensured, using the Lyapanov stability theorem. To verify the robustness properties of the closed-loop system, with respect to the input voltage variation and load resistance, some simulation studies are presented and discussed. The results show that power losses should be considered in the controller design for an HPS. The experimental results, by implementation on SPARTAN XC3S400 chip, are also given for justification.

Keywords- Sliding mode control (SMC), load resistance, power losses, hybrid power source (HPS), photovoltaics (PV).

1. Introduction

Among renewable energy resources, photovoltaic (PV) energy has been received more attention with many feasible applications, as it is free, abundant, and environmental friendly [1, 2]. The application of PV arrays in stand-alone systems has become popular due to some advantages [3], as low upkeep cost, low maintenance, no waste or byproducts, and easy expansion by using multiple solar panels and batteries.

The output power of a PV panel relies on solar irradiance levels. For instance, at night, a PV panel cannot produce any power [4]. Therefore, when solar energy is available, a PV converts it into electrical energy, then the boost converter is used to transmit the maximum power to the load, the surplus power of the load is transmitted to the battery by the bi-directional converter that acts as a buck converter, and the battery is charged. When there is no solar energy or low, the bi-directional converter acts as a boost converter and transmits the battery power to the load. Therefore, hybrid power sources (HPSs) are designed to generate power more efficiently [5].

Recently, the problem of controlling HPS has been studied and reviewed [5-9]. The APBC controller has designed by using algebraic parameter identification [5-6]. The method introduced, regarding the algorithm, the control signal cannot be followed by rapid changes, the changes must be slow, and therefore the dynamic response of the system is slow and is accompanied by a large overshoot. Two PI control loops to control the hybrid system is used [7]. Then it uses sliding mode control for the same system. The results show that the PI based control system is not able to maintain its good response when the operation point is not inside a limited range around the operating point selected to design the controllers. Due to the characteristics of the HPS and the microgrid operation, the PI based controller cannot assure the stability of the system in the entire operation range and consequently is not an acceptable option for this application. The sliding mode controller shows a higher robustness and it is able to operate correctly at the different cases that have been analyzed. The SMC is designed for the conventional model of HPS [8-10], but the problem that it enters is that the dynamical equations of the system are considered ideal and power losses such as_

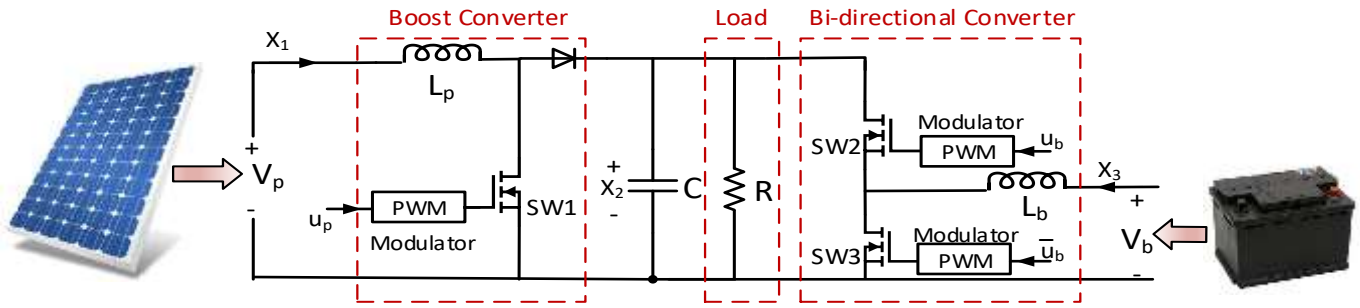

Fig. 1. Circuit diagram of HPS.

loss of inductors and losses of power switches in the converter for battery current designing are not considered; therefore, this causes the lack of proper dynamic response is desirable, and there is always an error in the system with respect to the amount of losses. Particularly, with increasing power consumption or increasing the switching frequency in these systems, the losses of the converters will also increase [11].

Although various constructions have been proposed to reduce losses, it should be noted that this will make the converter more complex, more expensive and more difficult to control. In this article, we'll see if the power losses in the design of SMC to consider or ignore, what would be the results. The purpose of this paper is to design a control signal with the ability to guarantee the stability to adjust the output voltage to the desired value, taking into account power losses in the converter. It is expected that this algorithm can provide a fast dynamic response and reduce the effect of disturbances (load, temperature, and radiation intensity) while guaranteeing sustainability.

2. System Modeling

The circuit modules of an HPS schematically are shown in Fig. 1. The system consists of a PV panel, a battery and interfacing DC-DC converters, i.e., a boost converter and a bi-directional converter.

The equivalent circuitry of a PV cell is shown in Fig. 2, in which the simplest model can be represented by a current source in antiparallel with a diode and the non-idealities are represented by the insertion of the resistances R_s (series resistance) and R_p (parallel resistance).

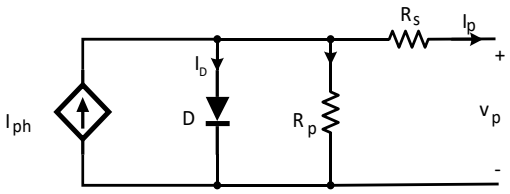

Fig. 2. Equivalent model of the PV panel.

The PV panel simulation model is based on the output current of one PV equivalent model, and its mathematical equation [5,12] is represented by:

$$I_p = I_{ph} - I_{rs}\left(e^{\frac{q(V_p+I_pR_s)}{Ak_bT}} - 1\right) - \frac{(V_p+I_pR_s)}{R_p} \quad (1)$$

$$I_{ph} = \frac{\lambda}{1000}[I_{scr} + k_l(T - T_r)] \quad (2)$$

$$I_{rs} = I_{or}\left(\frac{T}{T_r}\right)^3 e^{\left(\frac{qE_g}{k_bA}\left(\frac{1}{T_r}-\frac{1}{T}\right)\right)} \quad (3)$$

where V_p and I_p are the PV cell voltage and current, respectively, I_{rs} is the diode reverse saturation current, q is the electron charge (1.6×10^{-19} coulomb), A is the ideality factor of the p-n junction (1.12), k_b is the Boltzmann constant (1.3805×10^{-23} J/K), $\boldsymbol{\lambda}$ is solar irradiance level (0~1000 W/m2), k_l is the temperature coefficient (12×10^{-4}A/K), T is the cell temperature, T_r is the reference temperature (298°K), E_g is the bandgap energy (1.2ev), I_{or} is the saturation current at T_r (5.98×10^{-8} A), and I_{scr} is the short circuit current (1.45 A). Solar irradiation and temperature are strongly influenced by climate changes. Thus, it becomes necessary to use techniques to extract the maximum power from these panels. The requirement for maximum power point tracking (MPPT) is raised by the fact that the MPP of the PV panel continuously varies with temperature and illumination changes.

All of the possible modes of operation HPS are shown in Fig. 3. By utilizing the state-space averaging method [13], dynamic equations of the system can be expressed as:

$$\begin{cases} L_p\dot{x}_1 = V_p - (R_{lp} + R_{sw1})x_1 - (x_2 + V_D)(1 - u_p) \\ C\dot{x}_2 = -\frac{x_2}{R} + x_1(1 - u_p) + x_3u_b \\ L_b\dot{x}_3 = V_b - (R_{lb} + R_{sw3})x_3 - (x_2 + R_{sw2}x_3 - R_{sw3}x_3)u_b \end{cases} \quad (4)$$

where L_p and L_b denote the inductances, C is the capacitor, R is the load resistance, R_{lb} and R_{lp} denote the resistance of the inductors L_b and L_p, respectively, the conductive resistances of switches are represented by R_{sw1}, R_{sw2} and R_{sw3}, V_p is the voltage of the PV panel and V_b denotes the voltage of the battery. $X = [x_1, x_2, x_3]^T$ is the state vector which includes current of the PV panel (I_p), load voltage (V_C) and battery current (I_b), respectively. The control inputs $0<u_p<1$ and $0<u_b<1$ are the duty cycle of the switches SW1 and SW2, respectively (SW3 acts in the opposite direction of SW2).

3. Controller Design

The goal of the controller is to produce two control signals, including u_p, applied to the boost converter for MPPT of the PV panel, and u_b, applied to the bi-directional converter for load voltage regulation with considering power losses in_

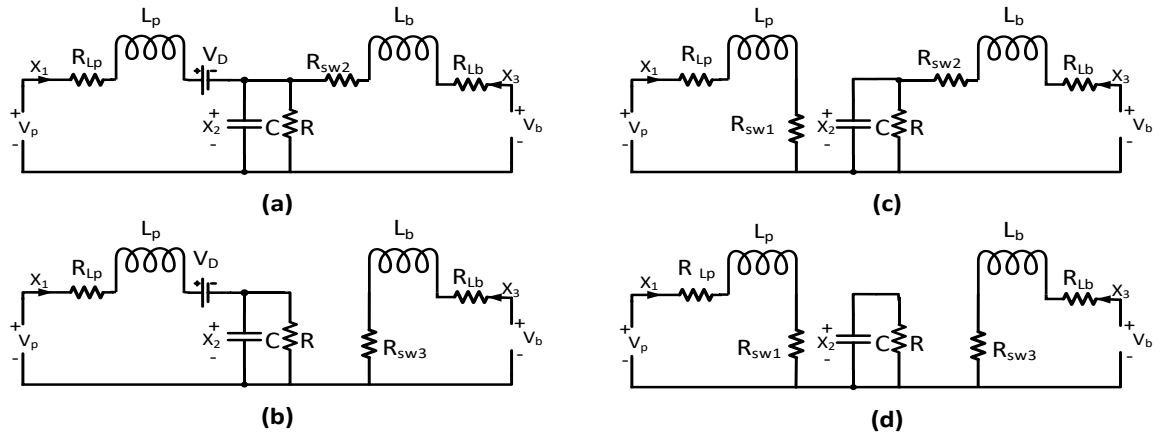

Fig. 3. Different modes of HPS. (a) sw1=O, sw2=C, sw3=O. (b) sw1=O, sw2=O, sw3=C. (c) sw1=C, sw2=C, sw3=O. (d) sw1=C, sw2=O, sw3=C. (open = O and close = C).

the converter. The design of two control signals in sections 3.1 and 3.2 is given, respectively. The main purpose of this paper is expressed in the sections 3.2 where it is related to the controller design for load voltage regulation with considering the power loss in the converter.

3.1. MPPT controller designer

Several studies have been carried out in the field of MPPT design, such as perturb and observe (P&O) [14-16], incremental conductance (INC) [17-18], adaptive control [19-20], neural networks [21], fuzzy logic [12, 22] and SMC [23]. INC with PI is adopted here, because the method that exhibits good performance [24] due to the high tracking factor (TF) and better adapt to the rapidly changing atmospheric conditions and it can be easily implemented due to the advancements of digital signal processors (DSP). The block diagram of this method is shown in Fig. 4.

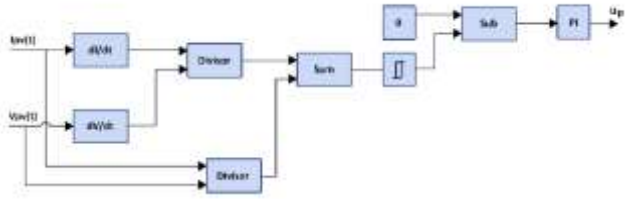

Fig. 4. Implementation of IC method using PI controller [24].

3.2. Load voltage regulation controller designer

A bidirectional DC/DC converter is used for load voltage regulation and charge or discharge the battery storage. In this section, we intend to adjust the load voltage to the desired value by designing a simple algorithm and using a sliding mode controller. It is expected that this algorithm can neutralize the effect of power loss in the converter, and thus the controller, while ensuring stability, generates fast dynamic response, reduces the effect of disturbances (load and temperature, and radiation intensity). Voltage regulation sliding surface (s) is selected as

$$s = x_3 - x_{3d} \tag{5}$$

where x_{3d} is the desired battery current. It can be described by:

$$p_b + p_{pv} = p_L + p_{loss} \tag{6}$$

$$x_3 = \frac{1}{v_b}\left(\frac{{x_2}^2}{R} - v_p x_1\right) + \frac{p_{loss}}{v_b} \tag{7}$$

where p_b, p_{pv}, p_L and p_{loss} are battery power, PV power, load power, and power losses respectively. P_{loss} includes all system losses such as power loss of inductors, switching and conduction losses of switches, etc.

Desired battery current can be described by:

$$x_{3d} = \frac{1}{v_b}\left(\frac{{x_{2d}}^2}{R} - v_p x_1\right) + \frac{p_{lossd}}{v_b} \tag{8}$$

where p_{lossd} is the desired power losses and it can be described by:

$$p_{lossd} = v_b(-k_p(x_2 - x_{2d}) - k_i \int (x_2 - x_{2d})dt) \tag{9}$$

where k_p and k_i are constant coefficients. By replacing (9) into (8):

$$x_{3d} = \frac{1}{v_b}\left(\frac{{x_{2d}}^2}{R} - v_p x_1\right) - k_p(x_2 - x_{2d}) - k_i \int (x_2 - x_{2d})dt. \tag{10}$$

Regarding equations (7) and (8) we have:

$$(x_3 - x_{3d}) - \frac{1}{v_b}(p_{loss} - p_{lossd}) = \frac{1}{v_b R}({x_2}^2 - {x_{2d}}^2) \tag{11}$$

when x_3=x_{3d} and p_{loss}=p_{lossd} , then $x_2 = x_{2d}$ and x_{3d} is ideally designed. In the conventional algorithm [8], p_{lossd} is not considered. In this case, even if the SMC can converge x_3 to x_{3d}, x_2 will not converge to x_{2d}, and the higher the power losses, the greater the output system error.

In order to get the equivalent control (u_{eq}), the equivalent control is determined from the following condition:

$$\dot{s} = \frac{\partial s}{\partial x_1}\dot{x}_1 + \frac{\partial s}{\partial x_2}\dot{x}_2 + \frac{\partial s}{\partial x_3}\dot{x}_3 = 0. \tag{12}$$

The equivalent control is then derived:

$$u_{eq} = \frac{v_b - (R_{lb} + R_{sw3})x_3}{x_2 + (R_{sw2} - R_{sw3})x_3}. \quad (13)$$

Since the range of duty cycle must lie in $0 < u_b < 1$, the real control signal is proposed as

$$u_b = \begin{cases} 0.05 & u_{eq} + k_s s \le 0.05 \\ u_{eq} + k_s s & 0.05 < u_{eq} + k_s s < 0.95 \\ 0.95 & 0.95 \le u_{eq} + k_s s \end{cases} \quad (14)$$

where k_s is constant coefficient and is determined by trial and error method by using computer simulations. The existence of the approaching mode of the proposed sliding function s is provided. A Lyapunov function v is positive definite term and defined as

$$V = \frac{l_b}{2} s^2. \quad (15)$$

The time derivative of V can be written as

$$\dot{V} = l_b s\dot{s}. \quad (16)$$

The achievability of s = 0 will be obtained by $\dot{V} < 0$. $\dot{V}$ can be written as follows:

$$\dot{V} = s[\, V_b - (R_{lb} + R_{sw3})x_3 - (x_2 + R_{sw2}x_3 - R_{sw3}x_3)u_b] \quad (17)$$

assumptions: $x_2 > v_b > 0$, $|v_b| > |x_3|$, $|R_{sw2} - R_{sw3}| < 1$, $k_s > 0$.

Three cases should be examined for the fulfillment of $\dot{V} < 0$.

Case I: For $u_b = 0.05$.

In this case x_3 is rising, as a result $L_b\dot{x}_3 > 0$, by replacing it into (1):

$$V_b - (R_{lb} + R_{sw3})x_3 - 0.05(x_2 + R_{sw2}x_3 - R_{sw3}x_3) > 0 \quad (18)$$

according to $u_{eq} + k_s s \le 0.05$, by replacing (12) it into:

$$V_b - (R_{lb} + R_{sw3})x_3 - .05(x_2 + R_{sw2}x_3 - R_{sw3}x_3) \le -k_s s(x_2 + R_{sw2}x_3 - R_{sw3}x_3) \quad (19)$$

by assumptions, $x_2 > R_{sw2}x_3 - R_{sw3}x_3$ and due to (18) the sign of s is negative, as a result due to the (17) and (18), $\dot{V}$ is negative definite.

Case II: For $0.05 < u_b < 0.95$.

By finding u_b from (14) and replacing (13), the following equation can be obtained:

$$\dot{V} = -k_s(x_2 + R_{sw2}x_3 - R_{sw3}x_3)(x_3 - x_{3d})^2 \quad (20)$$

since $(x_2 > (R_{sw2} - R_{sw3})x_3$, $\dot{V}$ is negative definite.

Case III: For $u_b = 0.95$.

In this case x_3 is falling, as a result $L_b\dot{x}_3 < 0$, by replacing it into equation (1):

$$V_b - (R_{lb} + R_{sw3})x_3 - 0.95(x_2 + R_{sw2}x_3 - R_{sw3}x_3) < 0 \quad (21)$$

in this case $u_{eq} + k_s s \ge 0.95$, by replacing (13) it into:

$$V_b - (R_{lb} + R_{sw3})x_3 - 0.95(x_2 + R_{sw2}x_3 - R_{sw3}x_3) \ge -k_s s(x_2 + R_{sw2}x_3 - R_{sw3}x_3) \quad (22)$$

since $(x_2 + R_{sw2}x_3 - R_{sw3}x_3) > 0$ and due to (21) the sign of s is positive , as a result due to (17) and (21), $\dot{V}$ is negative definite.

From the discussion above, the stability of the system can be guaranteed using the proposed control law (14). In order to obtain x_{3d} and u_b the values of x_1, x_2, x_3, V_b, V_p, V_{lb}, R, R_{sw2}, R_{sw3} and R_{lb} are required. To measure the first five parameters, we use the sensor and applied section C to calculate the last four parameters.

3.3. R, R_{lb}, R_{sw2} and R_{sw3} calculate

The PWM signals SW1 and SW2, load voltage (x_2) and battery current (x_3) shown in Fig. 5. Using the system modes previously described the value of R can be measured. In the mode (d) where SW1=close and SW2=open, capacitor c is discharged through the load resistor. It is sufficient to measure the load voltage (x_2) between the two specified times, then we have the capacitance discharge equation:

$$R = -\frac{t_R}{c(\ln x_2(t_R) - \ln x_2(0))} \quad (23)$$

this mode shown in Fig. 8 where $x_2(t_R)$ is the Capacitor voltage at time t_R, $x_2(0)$ denotes the initial voltage of the capacitor and t_R is the time at which the capacitor voltage from $x_2(0)$ to $x_2(t_R)$.

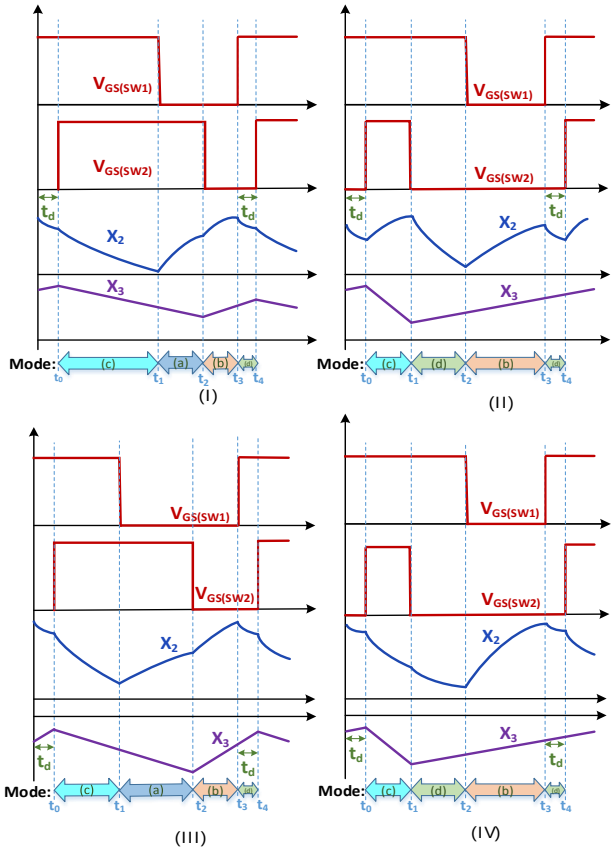

Fig. 5. Key operation waveforms of the proposed HPS when operating in (I) $u_p<u_b$, $x_3>0$, (II) $u_p>u_b$, $x_3>0$, (III) $u_p<u_b$, $x_3<0$, (IV) $u_p>u_b$, $x_3>0$.

To calculate R, it is necessary to create a delay of t_d size between the two PWM signals SW1 and SW2. If there is no delay, R may not be calculated. For example, in Fig. 5. (I) and 5. (III), if not delayed (t_d), R cannot be calculated because SW1=close and SW2=open, does not occur. $t_R<t_d$ shown in Fig. 6, because there will be a small spark in the load voltage and current on the rising and falling edge of the pulses.

The value of R_{lb} can be measured in any mode, for this purpose, a sensor is needed to measure the voltage (V_{lb}) of the L_b, then we have the inductance equation:

$$R_{lb}x_3 = V_{lb} - L_b\left[\frac{x_3(t_R)-x_3(0)}{t_R}\right]. \quad (24)$$

The value of R_{sw2} can be measured in the mode (a) or (c) where SW1=open or close and SW2=close, by using the law KVL:

$$R_{sw2}x_3 = V_b - V_{lb} - x_2. \quad (25)$$

The value of R_{sw3} can be measured. In the mode (b) or (d) SW1=open or close and SW2=open, by using the law KVL:

$$R_{sw3}x_3 = V_b - V_{lb}. \quad (26)$$

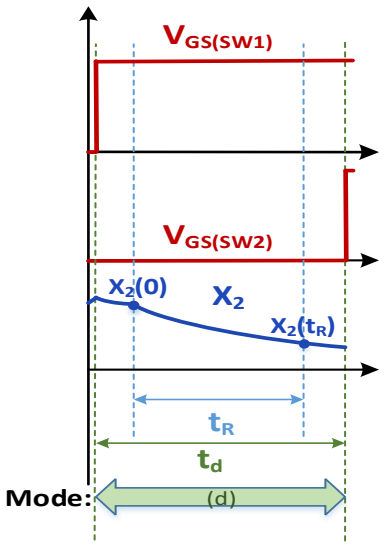

Fig. 6. Demonstration of mode (d) for calculating R

4. Simulation Results

MATLAB environment is used to investigate the performance of the proposed model and controller structure for HPS with considering power losses. The results are compared with the case of ignoring power losses .The simulation investigates two system characteristics: robustness against irradiance and load resistance changes. The profile of solar irradiance and load resistance are shown in Fig. 7. The specifications of the PV panel, DC converters, and parameters of the controller are shown in Table I. R_{lb}= R_{lp}=1.5Ω and R_{sw1} = R_{sw2} = R_{sw3} =0.077 Ω. The desired output voltage (x_{2d}) is 35 V and MPPT comes from INC with PI algorithm [24]. Fig. 8 shown the load voltage (x_2), it is observed that proposed control structure and model, tracks the reference value, but the conventional model and algorithm, in which power losses are ignored, due to the power losses, cannot set the output to the desired value. Fig .9 (b) shows that the battery current designed with the measured does not converge and the higher the power losses, the greater the non-convergence, due to the lack of accurate modeling of the system. However, if the system model is accurate and we do not consider losses in the design of the battery current, we will still be in error on the system output. Fig 10 and 11 shown PV voltage (V_p) and current (x_1), control signal (u_p), battery voltage (V_b) and current (x_3) and control signal (u_b) between the two cases, SMC with proposed algorithm and model, with conventional model and algorithm. It is clear from Fig .10 that in both cases, the MPP is well extracted.

Table. I. Parameters Description

Symbol	Comment	Value
P_{max}	Power maximum of the PV	16.2W
V_p	Output voltage of the PV	16.2v at p_{max}
X_1	Output current of the PV	1A at p_{max}
V_{oc}	Open circuit voltage of the PV	19.6V
I_{sc}	Short circuit current of the PV	1.45A
V_b	Battery voltage	12V-7Ah
L_b, L_p	Inductor	5mH
$F_{sw2,3}$	Switch frequency	31.25kHz
SW1,2,3	MOSFET switch	IRF540
C	Capacitor	470 µf
K_s	Constant coefficient SMC	0.8
K_p	Proportional coefficient	0.6
K_i	Integral coefficient	0.005
t_R	Sampling time	1µsec
t_d	Delay between the two PWM signals SW1 and SW2	1.4 µsec

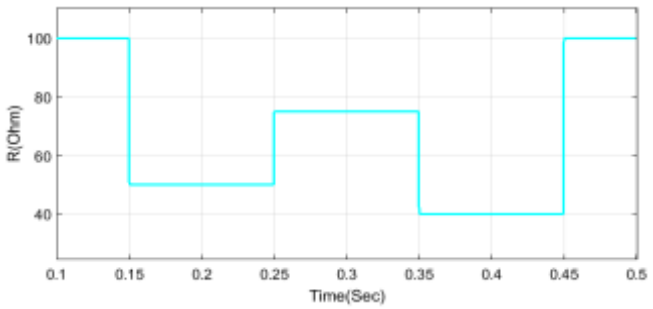

(a)

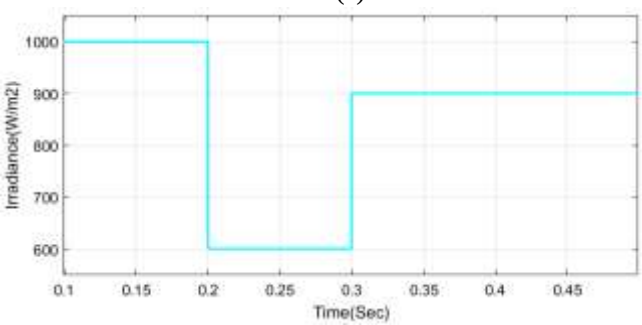

(b)

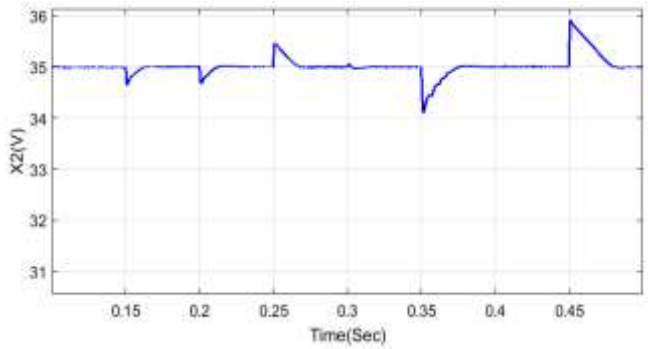

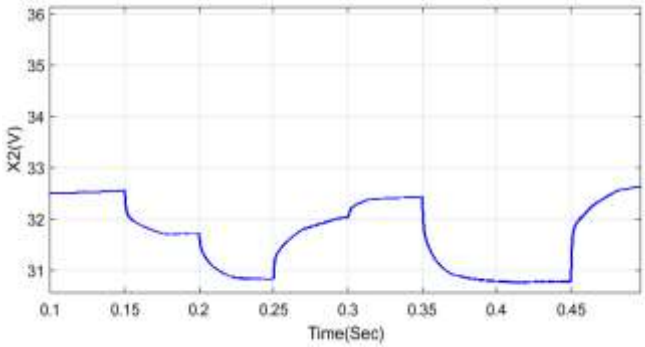

(a) (b)

Fig. 8. Load voltage (a) with proposed control structure and model and (b) with conventional algorithm and model.

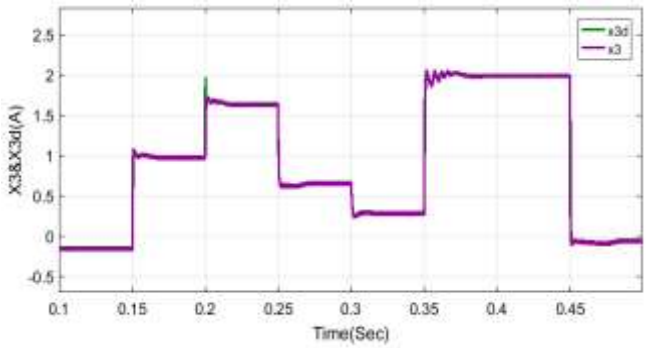

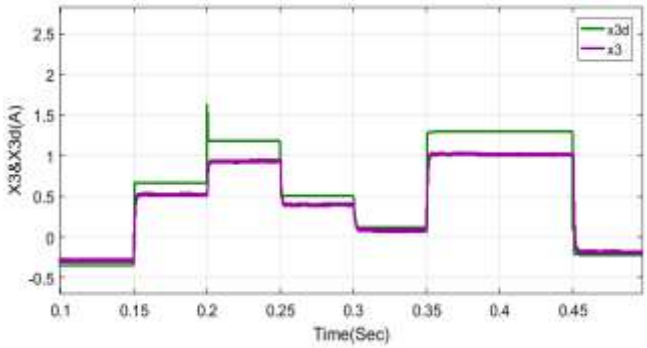

(a) (b)

Fig. 9. Battery current and desired (a) with proposed and (b) with conventional algorithm and model.

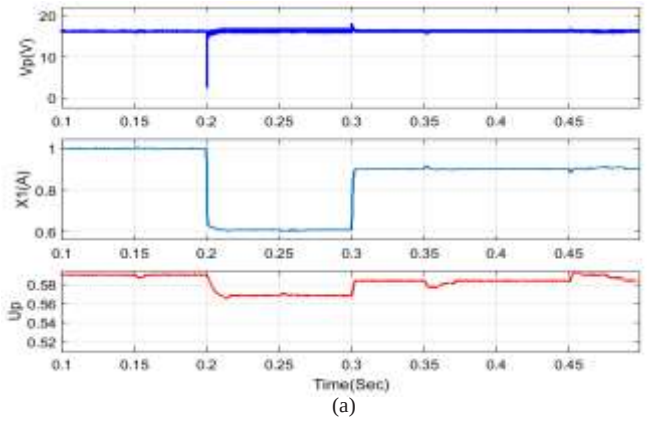

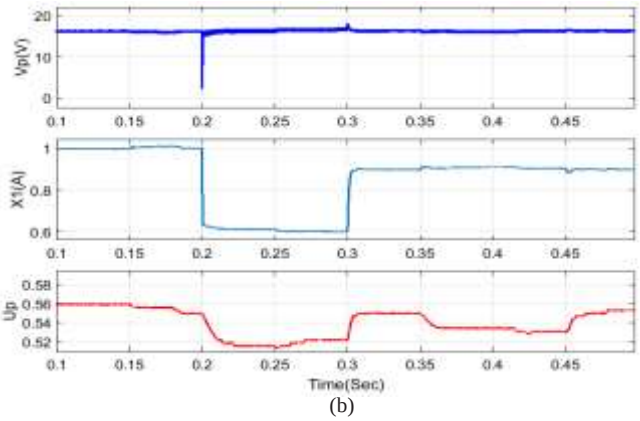

(a) (b)

Fig. 10. PV voltage and PV current and control signal u_p (a) with proposed and (b) with conventional algorithm and model.

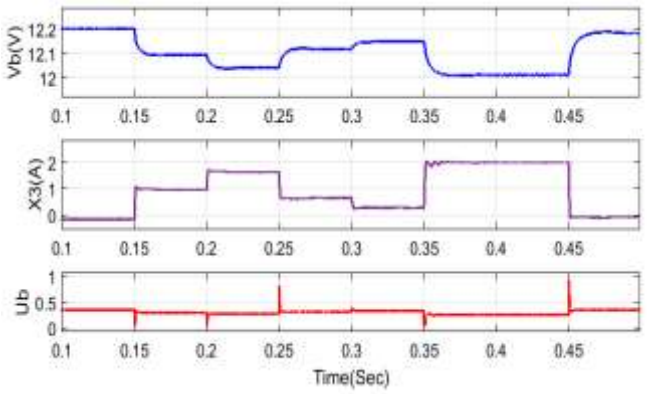

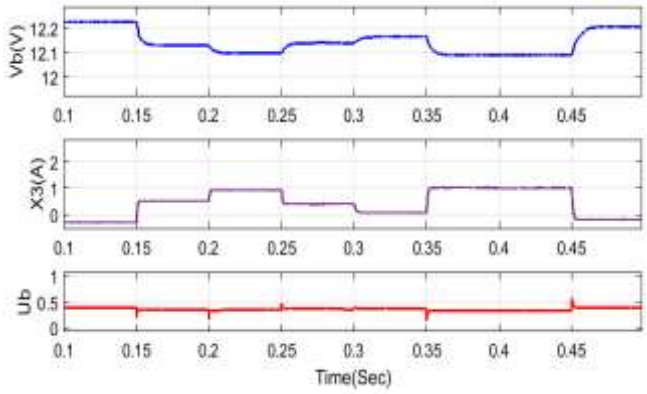

(b)

Fig. 11. Battery voltage and battery current and control signal u_b (a) with proposed and (b) with conventional algorithm and model.

Fig. 12 shows the power losses in various disturbances and verifies that the proposed model and algorithm are well suited for tracking system losses.

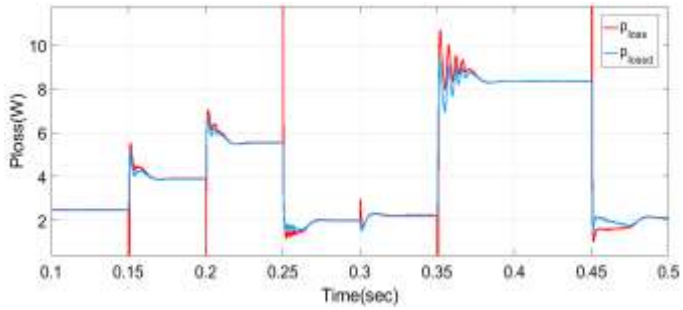

Fig. 12. Power losses in the converters

5. Experimental Validations

To verify the robustness of the controller with proposed model and algorithm, the experiment configuration is set up as shown in Fig. 13, where specifications of the system are shown in Table I. The proposed controller is implemented on SPARTAN XC3S400 chip. The PV voltage (V_p) and current (x_1), battery voltage (V_b) and current (x_3), the voltage of the L_b (V_{lb}) and load voltage (x_2) are sent to the A/D pins of the chip. Afterward, the control signals (u_p and u_b) are calculated and then, a PWM signal at 31250 Hz is directly generated to control the switches of the HPS. A block diagram of the experimental setup is shown in Fig. 18.

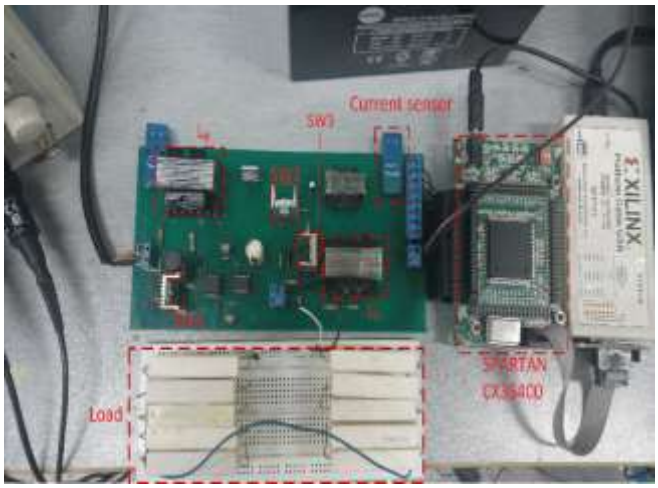

Fig. 13. Implementation of the closed-loop system

The control objectives are load voltage regulation to 35 V, the PV irradiance is 1000 W/m2 and the temperature is 298°K and at MPPT, V_p=16.2v, x_1=1A. In order to verify the estimation and tracking ability of the system, we using a photovoltaic panel emulator [25]. The resistance of the load varies directly from 50 to 100 Ω, and vice versa. Fig. 14 shows the voltage and current of the load unit. The first transient corresponds to load variation from 50 to 100 Ω, and the last transient corresponds to load variation from 100 to 50 Ω. It can be seen that the SMC with a proposed equation for designing the battery current and model is able to track the reference voltage of the load with a reasonable performance, regardless of the load variation. The load disturbance produces a maximum transient deviation of the load voltage below 4%, which is rejected in less than 25 ms. Afterward, the load voltage returns to 35 V after a fast transient state. Fig. 15 shows the battery current. It can be seen that when the load resistance is increased from 50 to 100 Ω, the required power is lower than the PV power. In this condition, the sign of the battery current is negative. Fig. 16 presents the PV current (x_3). It can be observed that the proposed INC MPPT with PI regulates the PV current to I_{mppt} without steady-state error. The settling time of the PV current (x_3) is about 25 ms. This tracking performance can maximize the extracted PV power. Experimental waveforms of the PV and battery voltages are shown in Fig. 17. It can be observed that the PV voltage is nearly constant, while the battery voltage exhibits high variation due to the internal resistance. In the charge state, the battery voltage is higher than the nominal voltage. It can be concluded that the proposed system is robust with respect to PV voltage variation. Moreover, since the voltage of the battery changes due to the internal resistance, the proposed system is also robust toward battery voltage variations.

Fig. 14. Transient response with the load resistor (R) varying periodically stepwise between 50 and 100 Ω. CH1 (Bottom) load current (200 mA/div). CH2 (Top) load voltage (5V/div). Load voltage tracks the desired 35-V reference well.

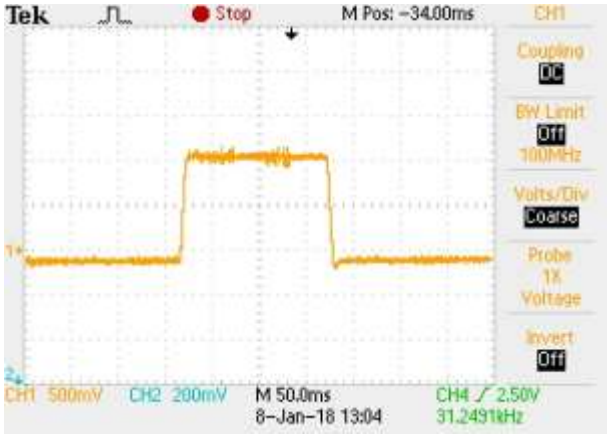

Fig. 15. Transient response with the load resistor (R) varying periodically stepwise between 50 and 100 Ω. CH1: battery current (x_3) (500 mA/div).

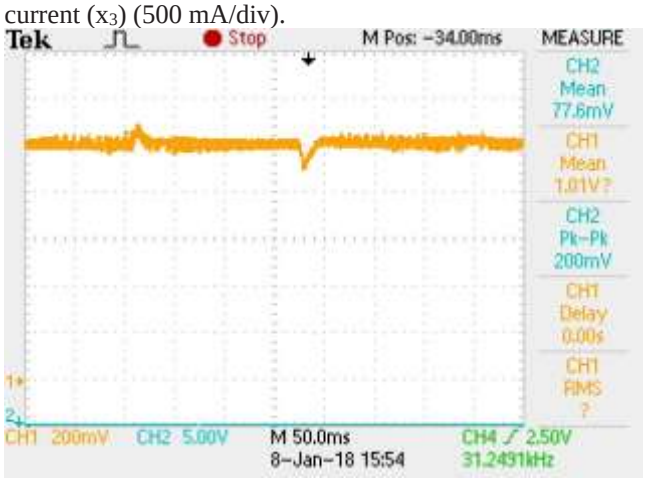

Fig. 16. Transient response with the load resistor (R) varying periodically stepwise between 50 and 100 Ω. CH1: Pv current (x_1) (200 mA/div).

Fig. 17. Transient response with the load resistor (R) varying periodically stepwise between 50 and 100 Ω. CH1 (Top) battery voltage (V_b) (5 V/div). CH2 (Bottom) PV voltage (V_p) (5 V/div).

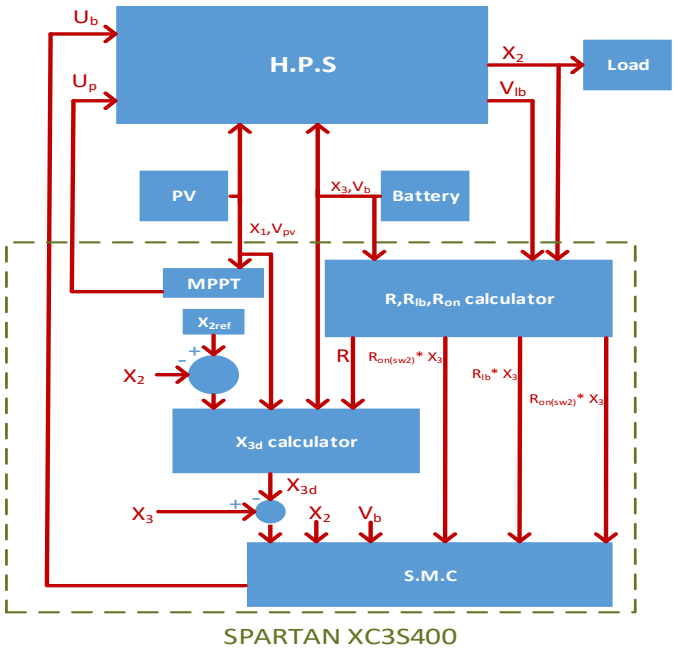

Fig. 18. Block diagram of the experimental setup.

6. Conclusion

This paper the role of taking into account power losses in the design of sliding mode controller for HPS system has been presented. For this purpose, the exact system model was provided with a relationship for designing the battery current. To investigate the validity of the proposed model and control structure, we compared the HPS once, regardless of power losses, and once more with regard for power losses by the SMC controller. Simulation and experiment results show that the proposed system is robust to input voltage variations and load changes. The proposed system tracks the reference values well, because, the proposed system tracks battery current and power losses. Conventional model and algorithm that do not consider power losses in the system, cannot accurately estimate battery current and in lead to a lack of proper dynamic response.

References

[1] E. F. Fernández, F. Almonacid Cruz, T. K. Mallick, and S. Sundaram, "Effect of Spectral Irradiance Variations on the Performance of Highly Efficient Environment-Friendly Solar Cells", IEEE J. Photovoltaics, vol. 5, Issue. 4 , pp. 1150–1157, Jul. 2015.

[2] K. Kumar, N. Ramesh Babu, K. R. Prabhu, "Design and Analysis of an Integrated Cuk-SEPIC Converter with MPPT for Standalone Wind/PV Hybrid System", International Journal of Renewable Energy Research, Vol.7, No. 1, pp. 96-106, 2017.

[3] A. Mills and R. Wiser, "Changes in the economic value of photovoltaic generation at high penetration levels: A pilot case study of California", IEEE J. Photovoltaics, vol. 3, no. 4, pp. 1394–1402, Oct. 2013.

[4] K. Sauer, T. Roessler, and C. Hansen, "Modeling the irradiance and temperature dependence of photovoltaic modules in PVsyst", IEEE J. Photovoltaics, vol. 5, no. 1, pp. 152–158, Jan. 2015.

[5] M. R. Mojallizadeh and M. A. Badamchizadeh, "Adaptive Passivity-Based Control of a Photovoltaic/Battery Hybrid Power Source via Algebraic Parameter Identification", IEEE J. Photovoltaics, Vol. 6, pp. 532–539, Mar. 2016.

[6] A. Tofighi and M. Kalantar, "Power management of PV/battery hybrid power source via passivity based control", Renewable Energy, vol. 36, pp. 2440–2450, Sep. 2011.

[7] A. Etxeberria, I. Vechiu, H. Camblong, J.-M. Vinassa, " Comparison of Sliding Mode and PI Control of a Hybrid Energy Storage System in a Microgrid Application", Energy Procedia, vol. 12, pp. 966-974, Dec. 2011.

[8] M. R. Mojallizadeh, B. Karimi, "Nonlinear control of a satellite power system based on the sliding mode control", ISRN Aerospace engineering [Online]. Available: http://dx.doi.org/10.1155/2013/253564.

[9] N. S. Khabbazi, A. R. Vali, V. Behnamgol, "Control of a Photovoltaic/Battery hybrid power source using the algorithm Super Twisting", J. Engineering education (IJEE), Vol. 9, No. 2, Apr. 2017.

[10] M. R. Mojallizadeh, B. Karimi, "Nonlinear Control of a Photovoltaic/Battery Hybrid Power System, Based on the Sliding Mode Control", Iranian electric industry. J. Quality and productivity, Vol. 2, pp. 30–40, Apr. 2014.

[11] S. Dusmez, A. Hasanzadeh, A. Khaligh, "Loss analysis of non-isolated bi-directional DC/DC converters for hybrid energy storage system in EVs", Ind. Electronics (ISIE), 2014 IEEE 23rd International Symposium on.

[12] U. Yilmaz, A. Kircay, S. Borekci, "PV system fuzzy logic MPPT method and PI control as a charge controller", Renewable and Sustainable Energy Reviews, Vol. 81, Part 1, pp. 994–1001, Jan. 2018.

[13] A. Emadi, "Modeling and analysis of multi converter dc power electronic systems using the generalized state-space averaging method", IEEE Trans. Ind. Electron, vol. 51, no. 3, pp. 661–668, Jun. 2004.

[14] M. A. Elgendy, B. Zahawi, and D. J. Atkinson, "Operating Characteristics of the P&O Algorithm at High Perturbation Frequencies for Standalone PV Systems", IEEE Trans. Energy Conversion, Vol. 30, pp. 189–198, Mar. 2015.

[15] M. A. Abdourraziq, M. Ouassaid, M. Maaroufi, S. Abdourraziq, "Modified P&O MPPT technique for photovoltaic systems", 2013 International Conference on Renewable Energy Research and Applications (ICRERA), pp.728–733, 20-23 Oct. 2013.

[16] J. Ahmed and Z. Salam, "A Modified P&O Maximum Power Point Tracking Method With Reduced Steady-State Oscillation and Improved Tracking Efficiency", IEEE Trans. Sustainable Energy, Vol. 7, pp. 1506 – 1515, Oct. 2016.

[17] F. Liu, S. Duan, F. Liu, B. Liu and Y. Kang, "A Variable Step Size INC MPPT Method for PV System", IEEE Trans. Electron, Vol. 55, Jul. 2008.

[18] H. Hsieh , S. Shih , J. Hsieh , G. Hsieh, "A study of high-frequency photovoltaic pulse charger for lead-acid battery guided by PI-INC MPPT", 2012 International Conference on Renewable Energy Research and Applications (ICRERA), pp.1–6, 11-14 Nov. 2012.

[19] K. S. Rajesh, S. S. Dash, Bayinder, R. Sridhar, Ragam Rajagopal, "Implementation of an adaptive control strategy for solar photo voltaic generators in microgrlds with MPPT and energy storage", 2016 International Conference on Renewable Energy Research and Applications (ICRERA), pp.766–771, 20-23 Nov. 2016.

[20] H. Koofigar, "Adaptive robust maximum power point tracking control for perturbed photovoltaic systems with output voltage estimation", ISA Trans. , Vol. 60, pp. 285-293, Jan. 2016.

[21] Syafaruddin, E. Karatepe, and T. Hiyama, "Performance enhancement of photovoltaic array through string and central based MPPT system under non-uniform irradiance conditions", Energy Conversion and Management, vol. 62, pp. 131–140, Oct. 2012.

[22] S. Choudhury, P. K. Rout, "Adaptive Fuzzy Logic Based MPPT Control for PV System under Partial Shading Condition", International Journal of Renewable Energy Research, Vol.5, No. 4, pp. 1252-1263, 2015.

[23] S. Kahla, Y. Soufi, M. Sedraoui, M. Bechouat," Maximum Power Point Tracking of Wind Energy Conversion System Using Multi-objective grey wolf optimization of Fuzzy-Sliding Mode Controller", International Journal of Renewable Energy Research, Vol.7, No. 2, pp. 926-936, 2017.

[24] M. A. G. de Brito, L. Galotto, Jr., L. P. Sampaio, G. de Azevedo e Melo, and C. A. Canesin, "Evaluation of the Main MPPT Techniques for Photovoltaic Applications",

IEEE Trans. Ind. Electronics, vol. 60, no. 3, pp. 1156–1167, Mar. 2013.

[25] D. D. C. Lu and Q. N. Nguyen, "A photovoltaic panel emulator using a buck-boost dc/dc converter and a low cost micro-controller," Sol. Energy, vol. 86, no. 5, pp. 1477–1484, May. 2012.